Available online at www.sciencedirect.com

SciVerse ScienceDirect

Acta Materialia 60 (2012) 6025–6032

Acta MATERIALIA

www.elsevier.com/locate/actamat

Elastic properties of face-centred cubic Fe–Mn–C studied by nanoindentation and ab initio calculations

S. Reeh [a,*], D. Music [a], T. Gebhardt [a], M. Kasprzak [a], T. Jäpel [b], S. Zaefferer [b], D. Raabe [b], S. Richter [c], A. Schwedt [c], J. Mayer [c], B. Wietbrock [d], G. Hirt [d], J.M. Schneider [a]

[a] Materials Chemistry, RWTH Aachen University, D-52056 Aachen, Germany
[b] Max-Planck-Institut für Eisenforschung GmbH, D-40237 Düsseldorf, Germany
[c] Central Facility for Electron Microscopy, RWTH Aachen University, D-52056 Aachen, Germany
[d] Institute of Metal Forming, RWTH Aachen University, D-52056 Aachen, Germany

Received 22 March 2012; received in revised form 10 July 2012; accepted 11 July 2012
Available online 16 August 2012

Abstract

We have studied experimentally and theoretically the influence of C and Mn content on the Young's modulus of Fe–Mn–C alloys. Combinatorial thin film and bulk samples were characterized regarding their structure, texture and Young's modulus. The following chemical composition range was investigated: 1.5–3.0 at.% C, 28.0–37.5 at.% Mn and 60.6–69.8 at.% Fe. The experimental lattice parameters change marginally within 3.597–3.614 Å with the addition of C and are consistent with ab initio calculations. The Young's modulus data are in the range of 185 ± 12–251 ± 59 GPa for the bulk samples and the thin film, respectively. C has no significant effect on the Young's modulus of these alloys within the composition range studied here. The ab initio calculations are 15–22% larger than the average Young's modulus values of the as-deposited and polished thin film at 3 at.% C. The comparison of thin film and bulk samples results reveals similar elastic properties for equivalent compositions, indicating that the applied research strategy consisting of the combinatorial thin film approach in conjunction with ab initio calculations is useful to study the composition dependence of the structure and elastic properties of Fe–Mn–C alloys. The very good agreement between the presented calculations and the experimentally determined lattice parameters and Young's modulus values implies that the here-adopted simulation strategy yields a reliable description of carbon in Fe–Mn alloys, important for future alloy design.

Keywords: Iron alloys; Sputtering; Elastic behaviour; Ab initio electron theory; Nanoindentation

1. Introduction

Mn-rich transformation-induced plasticity/twinning-induced plasticity (TRIP/TWIP) steels reveal outstanding mechanical properties combining high strength (>1000 MPa) and superior ductility (elongation to failure of >50%) [1,2]. These exceptional properties are due to dislocation glide, mechanical twinning and strain-induced ε- and α-martensitic transformations [1]. The formation of twins (TWIP effect) or multiple martensitic transformations (TRIP effect) under mechanical load is affected by the stacking fault energy (SFE), which is dependent on temperature and chemical composition [3,4]. The influence of SFE [4], temperature [4,5] and strain rate [5] on the deformation mechanisms and the interactions among the various deformation mechanisms of face-centred cubic (fcc) Fe–Mn–C steels has been studied in a number of papers [6,7].

In contrast the C-induced changes on the elastic properties of high Mn steels have not been studied systematically before.

* Corresponding author. Tel.: +49 241 80 25984; fax: +49 241 80 22295.
E-mail address: reeh@mch.rwth-aachen.de (S. Reeh).

1359-6454/$36.00 © 2012 Acta Materialia Inc. Published by Elsevier Ltd. All rights reserved.
http://dx.doi.org/10.1016/j.actamat.2012.07.038

For the binary fcc Fe–Mn random alloys elastic properties have been reported by Music et al. [8], Gebhardt et al. [9] and Cankurtaran et al. [10]. Even though these alloys are antiferromagnetic (AFM) with Néel temperatures well above room temperature, their elastic properties are well predicted using the disordered local moment (DLM) approach [8,9] to describe the magnetic configuration. With magnetically ordered configurations, such as AFM, the stiffness of these random alloys is overestimated due to lack of lattice softening [9]. However, there are no systematic data on the dependence of the Young's modulus values on the C concentration in ternary fcc Fe–Mn–C alloys.

In this paper, the influence of the C and Mn content on the Young's modulus of fcc Fe–Mn–C steel thin film synthesized by combinatorial sputter deposition is systematically investigated and compared to the same data obtained from bulk samples. Ab initio calculations are carried out to determine the Young's modulus of selected Fe–Mn–C alloys and to correlate these with the electronic structure.

2. Experimental section

2.1. Thin film samples

The Fe–Mn–C thin films were grown by DC combinatorial magnetron sputtering. The depositions were carried out in a high vacuum chamber with a base pressure of 1.1×10^{-5} Pa using a system described in Ref. [9]. Fe, $Fe_{50}Mn_{50}$ and C targets, with 99.95% purity for Fe and $Fe_{50}Mn_{50}$ and 99.999% purity for C, were placed on three magnetrons. Magnetron power densities of 2.0, 3.2 and 0.5 W cm^{-2} were applied, respectively. The sputtering gas was Ar (99.9999% purity) and the pressure during deposition was 0.8 Pa. The substrate was a 2 in. sapphire wafer with a (0 0 0 1) orientation, which was heated to 450 °C during deposition. The substrate-to-target distance was ~10 cm. The Young's modulus values were determined in the as-deposited state with a root mean square roughness (R_q) of 57 nm; after polishing the R_q value was 15 nm, measured on an area of 94.2 μm × 70.7 μm.

2.2. Bulk samples

Two different types of bulk samples were produced: sample type A (A1, A2 and A3) and sample type B (B1, B2 and B3). The differences between these specimen sets are that the samples were produced in different ways (see below) and that samples B contain impurities of Al, S, P, Si, Cr, Ni, Mo, Cu, Co, Nb, V, Sn and N, which are typically introduced during large scale steel processing, while the samples A contain no detectable amounts of these impurities. The compositions of all bulk samples are given in Table 1. This experimental strategy allows for a direct comparison of the data obtained from bulk and thin film samples with results from ab initio calculations. Furthermore, the comparison between bulk specimens with and without impurities may shed light on the role of impurities for the Young's modulus and structure evolution.

For samples A, Fe (99.998% purity), Mn (99.99% purity) and C powders (99.9999% purity) were mixed and inductively melted. The melting was done in an inert atmosphere with a heating rate of 6 K s^{-1} from room temperature up to 1520 °C. The dwelling time at this temperature was 4 min, followed by cooling at a rate of 50 K s^{-1}. Samples with a diameter of 5 mm were mounted in conductive resin and subsequently polished to a roughness R_q of 19 nm for A1, 14 nm for A2 and 32 nm for A3 measured on an area of 94.2 μm × 70.7 μm.

The three samples, B, B1, B2 and B3, were cast in a vacuum induction melter at 1550 °C and solidified as slabs with a 140 × 140 mm^2 cross-section and a weight up to 100 kg. These samples were then processed into hot strips, starting with forging at 1150 °C with 60% thickness reduction, followed by rolling down at 1150 °C to ~3 mm thickness within 12 passes and an overall thickness reduction of 95%. The samples were cut into dimensions of 10 mm × 10 mm × 3 mm, mounted in conductive resin and polished to a roughness R_q of 16 nm for B1 and B2 as well as 20 nm for B3 measured on an area of 94.2 μm × 70.7 μm.

2.3. Analysis

2.3.1. Chemical composition

The chemical composition of the thin film and the bulk samples was measured using wavelength-dispersive spectroscopy (WDS) in a CAMEBAX SX 50 electron probe microanalyser. A focused electron beam of 15 keV with a current of 80 nA was used. The dwell time for each measured position was 10 s. The characteristic X-ray intensities were calibrated by using the following standards: Fe_3C, Mn and Fe. The calibrated intensities (k-ratios) were transferred into elemental concentrations with the help of a matrix correction procedure based on a special PHI (rhoz)-method, the so-called PAP correction procedure. Under the chosen conditions the sensitivity of the measurement is 0.23 at.% for C, 0.02 at.% for Mn and 0.03 at.% for Fe.

2.3.2. Structure and crystallographic texture analysis

The structure of the thin films was determined by X-ray diffraction in a Bruker D8 with a general area detection diffraction system (GADDS) with Cu Kα radiation at a constant angle of incidence of 15° with a 0.5 mm collimator covering a 2θ range of 35–85°. The structure of the bulk samples was measured by using a Siemens D5000 diffractometer using line-focused Cu Kα radiation in Bragg–Brentano beam geometry.

The electron backscatter diffraction (EBSD) technique was employed to analyse the local crystallographic texture in conjunction with the microstructure. In this study, EBSD for the bulk samples was carried out in a high-resolution, high-beam current field emission scanning electron

Table 1
Chemical composition of the bulk samples in at.%.

Sample	Fe	C	Mn	Si	P	S	Cr	Ni	Mo	Al	Cu	Co	Nb	V	Sn	N
A1	74.4	1.5	24.1	–	–	–	–	–	–	–	–	–	–	–	–	–
A2	74.0	1.2	24.8	–	–	–	–	–	–	–	–	–	–	–	–	–
A3	76.1	0.6	23.3	–	–	–	–	–	–	–	–	–	–	–	–	–
B1	75.4	2.4	21.8	0.219	0.013	0.005	0.018	0.032	0.011	0.015	0.009	0.007	0.013	0.017	<0.0002	0.058
B2	69.7	1.3	27.8	0.200	0.015	<0.001	0.017	0.034	0.011	0.011	0.008	0.010	0.016	0.022	<0.0002	0.062
B3	74.8	1.4	22.6	0.128	0.013	0.002	0.017	0.034	0.008	0.011	0.009	0.009	0.015	0.012	<0.0002	0.043

microscopy (SEM) instrument (JEOL JSM 6500F). Pattern acquisition was done using a DigiView II CCD camera by TSL and the TSL OIM data collection software. Orientation information was acquired on a hexagonal grid, using a step size in the range of 50–100 μm. EBSD maps were measured at 15 kV acceleration voltage and a working distance of 15 mm.

The EBSD measurement for the thin film was performed using a DigiView III camera by EDAX-TSL attached to a JSM 7000F FEG-SEM by JEOL operating at a beam current of ~10 nA and a beam energy of 20 keV.

The measured diffraction patterns were evaluated using the software OIM Data Collection V 6.1.3 indexing the patterns as fcc, body-centred cubic (bcc) or hexagonal-close-packed (hcp) Fe. In total, a field of 20 μm × 30 μm was mapped at an EBSD step size of 50 nm at a position with 64.7 at.% Fe, 33.7 at.% Mn and 1.6 at.% C.

2.3.3. Young's modulus

The Young's modulus was investigated with a depth-sensing nanoindenter (Hysitron TriboIndenter™) equipped with a Berkovich tip. The Young's modulus values were evaluated according to the Oliver and Pharr method [11] using a Poisson ratio of 0.25 [9]. The tip was calibrated on fused silica.

For the as-deposited thin film, measurements at 22 different positions with 12 indents per position and a maximum load of 1500 μN were performed. The maximum penetration depth was less than 10% of the film thickness. After polishing of the thin film, nine positions were measured again to evaluate the influence of roughness on the measurements, with 16 indents per position with indentation depth less than 100 nm at a film thickness of 1.2 μm.

The elastic properties of samples A1, A2 and A3 were measured using 72 indents per sample and samples B1, B2 and B3 were subjected to 32 indents per sample, using the same maximum load as for the thin films.

3. Theoretical section

The theoretical work was carried out using density functional theory [12], as implemented in the Vienna ab initio simulation program (VASP) [13,14]. The VASP code was applied to four chemically disordered alloys with AFM 3Q configurations with 24.2 at.% and 36.4 at.% Mn for ternary Fe–Mn–C with 3 at.% C, respectively as well as 25.0 at.% and 37.5 at.% Mn for binary Fe–Mn. This non-collinear AFM configuration is one of the ground state configurations proposed for Mn-rich steels [15,16] and provides a reliable description of the magnetic state to determine the elastic properties of these materials [9]. Even though the DLM approach gives rise to the best description of elasticity of Fe–Mn, it is not straightforward to apply it to alloys which contain interstitial elements. For the VASP simulations the projector augmented wavepotentials in conjunction with the generalized gradient approximation were employed [17]. The following parameters were applied: convergence criterion for the total energy of 0.01 meV, Blöchl corrections [18] for the total energy cut-off of 300 eV, and integration in the Brillouin zone according to Monkhorst-Pack [19] with 5 × 5 × 5 k-points. 2 × 2 × 2 supercells containing 32 atoms were created with randomly arranged positions of Fe and Mn following the special quasi-random structure (SQS) approach [20]. One C atom (3.0 at.%) was placed in the vicinity of Mn atoms at an interstitial position for Fe–Mn–C alloys, thus maximizing the number of Mn–C nearest neighbours, since this is reported to be the preferred lattice position [21]. The SQS implementation via the short-range order (SRO) parameter is available within the locally self-consistent Green's function (LSGF) software package [22,23]. The LSGF code was used to generate SQS supercells. The Warren–Cowley SRO parameter [24] was applied to account for randomness (less than 0.08 within five coordination shells). Electron density distributions were used to study the electronic structure of these AFM random alloys.

4. Results and discussion

The chemical composition of the thin film was analysed along line scans as illustrated in Figs. 1 and 2. The actual positions of the measurements are visualized as black dots. Based on these data the chemical composition was interpolated for the entire composition range. A compositional spread from 1.5 at.% up to 3.0 at.% C is observed in Fig. 1. In Fig. 2 the chemical composition for Fe and Mn is shown. The Fe content varies between 60.7 at.% and 69.8 at.%, while the Mn content lies between 28.0 at.% and 37.5 at.%.

The chemical composition of the bulk samples is given in Table 1.

We continue with discussing the structure. In Fig. 3a the X-ray diffractograms for compositions varying between 1.5 at.% and 2.8 at.% C at a Fe/Mn ratio of ~2.2 are

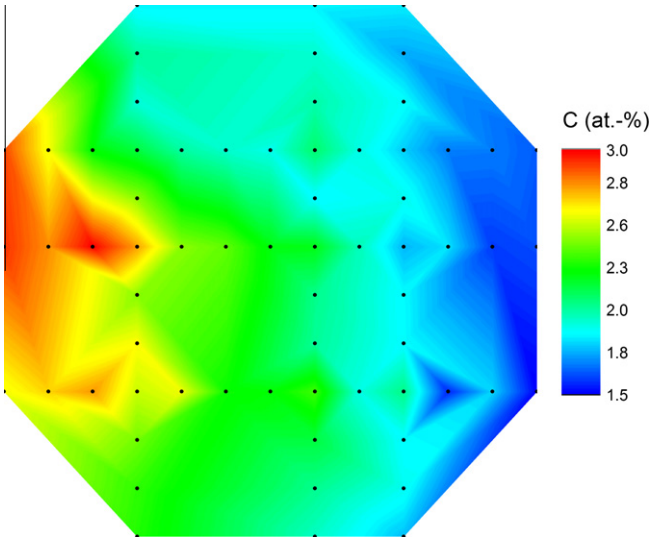

Fig. 1. C content of the thin film with the measured line scans (black dots); sample size is 51 mm diameter.

shown. For comparison the diffractograms reported by Gebhardt et al. [9] are shown in Fig. 3b. These earlier films from Gebhardt et al. [9] were grown without C, covering a Fe/Mn ratio of ~2.3. All peaks can be attributed to fcc structure austenite, indicating that the film is phase pure.

The lattice parameter was evaluated based on three peaks: (1 1 1), (2 0 0) and (2 2 0). Different positions on the combinatorial wafer with 28 at.%, 30 at.%, 33 at.% and 35 at.% Mn were chosen to determine the influence of C on the lattice parameter values. A comparison between the lattice parameter of thin film and bulk samples on the one hand and the VASP calculations on the other hand is shown in Fig. 4. The error bars display the standard deviation of the lattice parameter values. Experimental data for fcc Fe–Mn from Marinelli et al. [25] and for fcc $Fe_{57}Cr_{18}Ni_{15}Mn_{10}$ with additions of C from Gavriljuk et al. [26] as well as calculated data for fcc binary Fe–Mn alloys (DLM configuration) from Music et al. [8] are plotted for comparison. For the thin film the maximum C-induced lattice parameter change is 0.012 Å, corresponding to a 0.33% change in lattice parameter. The lattice parameter of the bulk samples is 3.600 ± 0.005 Å to 3.614 ± 0.001 Å, in the same range as those observed for the thin film, corresponding to a 0.39% change in lattice parameter, even though the Mn content differs. If one compares the average lattice parameter for the fcc ternary Fe–Mn–C thin film with the binary Fe–Mn data of Marinelli et al. [25] and Music et al. [8] the change in lattice parameter is 0.1% and 0.06%, respectively. For both bulk samples and thin film the effect of C on the lattice parameter is marginal. An influence of impurities (sum of all impurity elements is 0.4 at.%, see Table 1) on the lattice parameter of the bulk samples could not be observed for the composition range investigated here.

Ledbetter and Austin [27], Gavriljuk et al. [26], Shanina et al. [28] and von Appen and Dronskowski [21] reported a

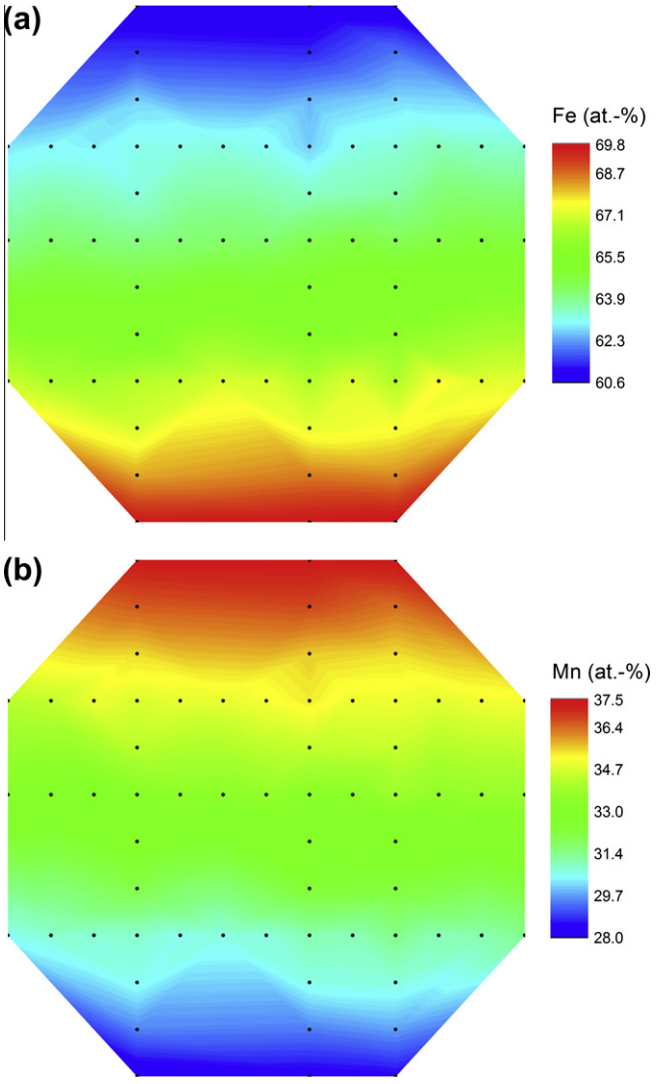

Fig. 2. Compositional spread of the thin film with the measured line scans (black dots) for (a) iron and (b) manganese content; sample size is 51 mm diameter.

lattice expansion caused by the incorporation of C into fcc iron-based alloys, but in each case only a small effect could be ascertained. Gavriljuk et al. [26] detected a lattice expansion of 0.008 Å, corresponding to a 0.22% change in lattice parameter with 2.1 at.% C in $Fe_{57}Cr_{18}Ni_{15}Mn_{10}$. Shanina et al. [28] reported an increase in the lattice parameter of 0.2% with 3.7 at.% C in $Fe_{56}Cr_{18}Ni_{16}Mn_{10}$, while the other authors did not quantify the reported increase in lattice parameter. Hence, the data reported here are consistent with the literature.

The ab initio calculations were carried out using the VASP code (AFM 3Q) for two different Fe/Mn ratios with a C content in the range between 0 and 3 at.%. The calculated data predict a small lattice expansion of 0.016 Å for 25 at.% Mn and 0.015 Å for 37.5 at.% Mn due to the addition of 3 at.% C. The lattice parameters predicted by the ab initio data underestimate the experimental data by $\leqslant 2\%$. For calculation results for configurations that are void of

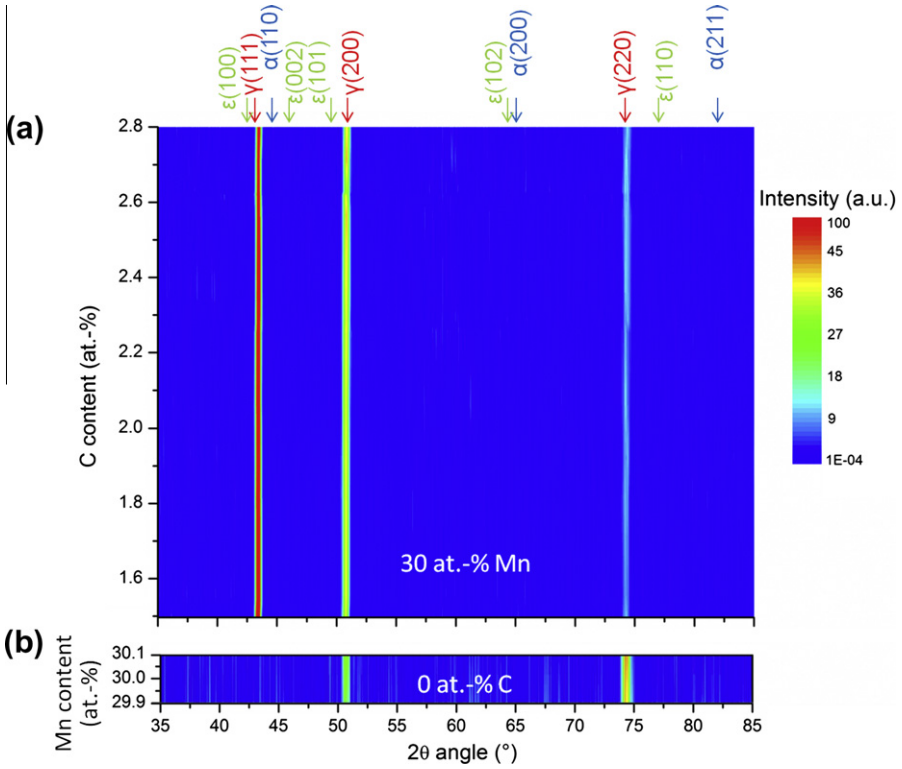

Fig. 3. Phase evolution of thin films vs. (a) C content for Fe/Mn of ~2.2 from this work and (b) Mn content for 0 at.% C taken from the data of Gebhardt et al. [9].

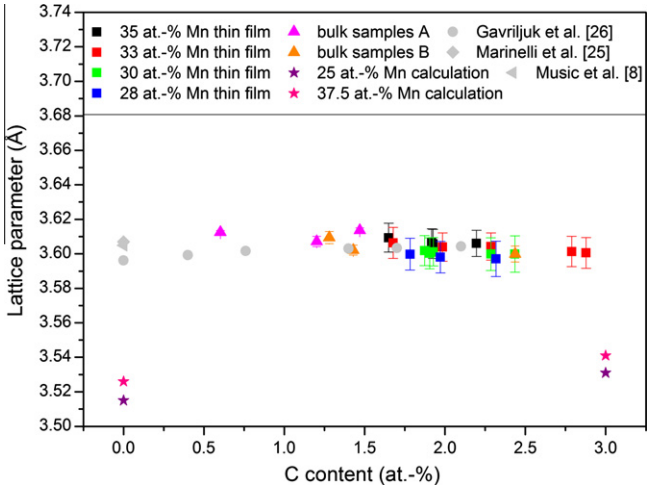

Fig. 4. Lattice parameter as a function of the C content for thin film (rectangles), bulk samples (triangles) and calculations (stars).

interstitial C the DLM method employed by Music et al. [8] yields good agreement with the experiments. It is evident that for the ternary system Fe–Mn–C, the experimental data are consistent with the theoretical predictions.

The crystallographic texture was analysed for the bulk and thin film samples. The EBSD measurements imply that the major phase is austenite for all samples. The microstructure of the samples A consists only of a few large grains: A1 exhibits an average grain size of ~2 mm, sample A2 of ~3 mm and sample A3 of ~5 mm. Most grains exhibit a subgrain structure stemming from solidification. The crystal orientations do not show any preference. The polished surfaces which were later used for modulus determination by nanoindentation show a large variety of different crystallographic surface normals. The samples of type B show average grain sizes which are much smaller than those of samples of type A: 106 μm for B1 and 70 μm and 60 μm for B2 and B3, respectively. They reveal a weak mixed copper-brass-type hot rolling texture with a maximum orientation density of about three times random (calculated via harmonic series expansion to a maximum rank of 34). This texture leads to a very slight preference of the [0 1 1] crystal direction parallel to the surface normal on the longitudinal cross-sections. These sections have been used to perform nanoindentation tests. This very weak preferred crystal direction should not significantly bias the results obtained from the nanoindentation on these surfaces. Sample A1 exhibits, besides the prevalent austenite phase, also hexagonal ε-martensite and tetragonal α′-martensite at the outer rim. Sample B3 shows ε-martensite at the outer rim. The martensite formation is in the current case caused by plastic deformation during manufacturing [29]. All experiments of the bulk samples were performed in the sample centre, where only the austenite phase was present. This ensures a meaningful comparison of the results obtained from the different bulk samples and those from the thin film. The grain scale texture information may be required for the correct interpretation of the nanoindentation results, especially for comparing the bulk data to the thin

film load–displacement indentation results in addition to the consideration of the chemical composition. Due to the small grain size of ~200 nm on average only 43% of the measured area on the thin film could be quantified with sufficient fidelity by EBSD. 99.8% of these indexable patterns indicate the presence of the austenitic phase; only 0.2% correspond to ε-martensite. The texture of the thin film has a slight preference in [0 0 1] and [1 0 2] crystal direction parallel to the surface normal. This very weak preferred crystal direction is expected not to influence the results obtained from the nanoindentation measurements.

The mechanical properties of the thin film and bulk samples were measured by nanoindentation. The resulting Young's modulus values for the thin films, bulk samples and calculations are plotted in Fig. 5 vs. the C concentration. The error bars show the standard deviation of the Young's modulus values. In Fig. 5a the measurements of the as-deposited thin film are shown, while in Fig. 5b the experimental data of the polished thin film are plotted. The average Young's modulus values of the as-deposited and polished thin films are in the same range, while the error bars are drastically reduced due to polishing. Calculated data (DLM configuration) of fcc Fe–Mn with an Fe/Mn ratio of 2.33 from Gebhardt [30] and experimental fcc $Fe_{60}Mn_{40}$ single-crystal data from Cankurtaran et al. [10] are plotted for comparison and are in a good agreement with both the experimental and theoretical data discussed here. For the thin films the Young's modulus values are between 188 and 251 GPa, while for the bulk samples these values range from 185 to 220 GPa. Both bulk sample types have similar Young's modulus values, even though samples B contain different levels of impurities. Thus, the impurities do not affect the Young's modulus within the compositional range based on the nanoindentation measurements. The Young's modulus values for the as-deposited thin films scatter by 24.6%. This is caused by the higher roughness value of the as-deposited thin film in comparison with the roughness of the polished bulk samples. Even though there are large error bars for the as-deposited thin film, the average Young's modulus values for thin film and bulk samples appear to agree rather well.

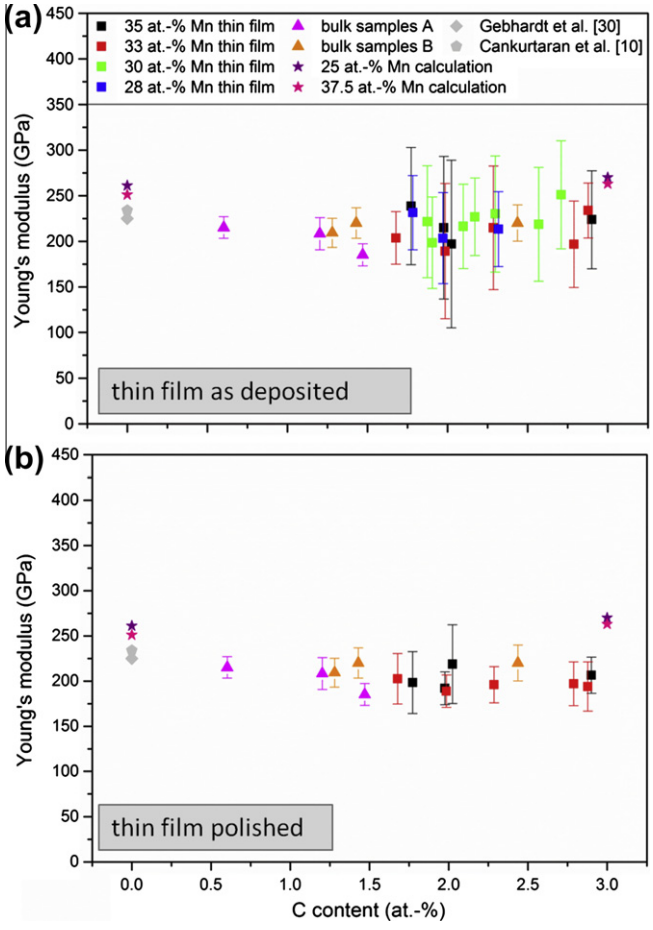

Fig. 5. Young's modulus as a function of C content for thin film (rectangles) and bulk samples (triangles) and calculations (stars) for (a) as-deposited thin film and (b) polished thin film.

Despite the different crystallographic textures and grain sizes of the bulk samples A and B, the experimental Young's moduli taken from the samples are similar. This may be due to the fact that the elastic anisotropy may not be quantified well using nanoindentation because during indentation in all directions of polycrystalline material the stiffness will be averaged [31,32]. The calculated elastic anisotropy of binary Fe–Mn with 37.5 at.% Mn and ternary Fe–Mn–C with 36.4 at.% Mn and 3 at.% C was 0.15 and 0.14, respectively. Thus, the change in elastic anisotropy with C addition is with 6.7% marginal.

Ledbetter and Austin [27] reported that a Young's modulus value reduced by 0.3% due to a 0.14–0.39 at.% C addition. This rather minute change is not quantifiable in the current indentation experiments. Hence, the current data are consistent with those in the literature, specifically in Ref. [27].

The VASP calculations of the elastic properties were conducted for four different compositions, see Fig. 5. These predicted values differ by 15–22% from the average experimental data at 3 at.% C for the as-deposited and polished thin film. Eriksson [33] reported that the calculated elastic properties can be determined within ~15% accuracy in comparison with the experiments. As the C concentration is increased to 3 at.%, the corresponding calculated Young's modulus increases by ~4%. While this increase is significant, it is too small to be verified in the current indentation experiments. Hence, the C changes considered in this work seem to have only a marginal influence on the overall Young's modulus values of fcc Fe–Mn–C alloys. This can be understood by considering the C-induced changes in the electronic structure.

In order to correlate the Young's modulus values with the electronic structure, we study the electron density distribution for the Fe–36.4 at.% Mn–3 at.% C alloy in comparison with the binary Fe–25 at.% Mn alloy in the crystallographic (0 0 4) plane of the fcc lattice structure (see Fig. 6). For the ternary Fe–Mn–C alloy the C atoms are located at the edges, while Fe and Mn are randomly

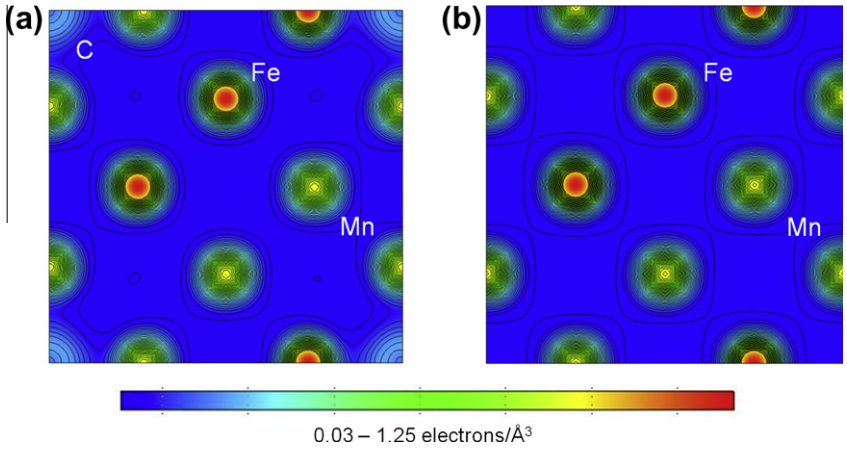

Fig. 6. Electron density distribution of (a) Fe–36.4 at.% Mn–3 at.% C and (b) Fe–25 at.% Mn in the (004) plane.

distributed at fcc sites within the SQS approach. The electron density never reaches zero in this plane, implying uniform distributions of charge between the metallic atoms. On the other hand, electrons are shared between C and the metals. Hence, the electronic structure can be described as a mixture of covalent (Fe–C and Mn–C) and metallic (Fe–Fe, Mn–Mn, Fe–Mn) bonding. According to von Appen and Dronskowski [21] the covalent bond is very strong, but it is not the most abundant one (3 at.% C in the Fe–Mn matrix). In other words, incorporation of C into the metallic matrix only leads to local effects so that no substantial changes in the electronic structure occur. Hence, C does not affect the Young's modulus to a larger extent in the concentration range investigated. This supports the presented experimental results.

5. Conclusions

The influence of the C and Mn concentration for austenitic Fe–Mn–C thin film and bulk samples on the Young's modulus and the equilibrium volume has been studied. Ab initio calculations have been carried out for selected alloy compositions using the VASP code. The calculated elastic property and equilibrium volume data were compared with experimental data to critically evaluate the reliability of the current design strategy for Fe–Mn–C alloys.

The experimental lattice parameter values vary in the whole composition range with C concentrations of 0–3 at.% by 0.017 Å. Hence, there is no significant dependence of the lattice parameter on the C concentration observed. The ab initio calculations predict that C expands the lattice slightly by 0.4% as compared to the binary metallic matrix. The ab initio calculations deviate by $\leqslant 2\%$ from the experiments and are hence in good agreement.

The C concentration does not have a significant influence on the Young's modulus of Fe–Mn–C alloys for the studied composition range. The measured Young's modulus values scatter for the polished thin film between 188 ± 18 GPa and 218 ± 43 GPa and for the bulk samples between 185 ± 12 GPa and 220 ± 20 GPa. The calculated Young's modulus values are 15–22% larger than the average Young's modulus values of the as-deposited and polished thin film at 3 at.% C. The Young's modulus values are in the same range for the as-deposited and polished thin film, while the experimental error is reduced on average from ~26% to ~13% as a result of polishing. The measured data for thin films and bulk samples as well as the calculated data reveal no significant influence of the C concentration on the Young's modulus. This is consistent with the observation of the absence of substantial changes in the electronic structure upon incorporation of C into the metallic matrix.

The thin film reproduces very well the properties of the bulk materials. Both thin film and bulk samples are probed in the austenite phase; lattice parameter data and Young's modulus values are in good agreement.

An influence of impurities of the bulk samples B could not be determined within the composition range investigated.

Thus both the presented implemented simulation strategy and the experimental approach are useful to predict and study the equilibrium volume and the Young's modulus of Fe–Mn–C alloys.

Acknowledgements

The authors gratefully acknowledge the financial support of the Deutsche Forschungsgemeinschaft (DFG) within the Collaborative Research Center (SFB) 761 "Steel – ab initio". The bulk samples A were provided by A. Lob from the Institute of Ferrous Metallurgy, RWTH Aachen University.

References

[1] Frommeyer G, Brüx U, Neumann P. ISIJ Int 2003;43:438.
[2] Gutierrez-Urrutia I, Raabe D. Acta Mater 2011;59:6449.
[3] Grässel O, Kruger L, Frommeyer G, Meyer LW. Int J Plast 2000;16:1391.
[4] Allain S, Chateau JP, Bouaziz O, Migot S, Guelton N. Mater Sci Eng A 2004;387:158.

[5] Bäumer A, Jimenez JA, Bleck W. Int J Mater Res 2010;101:705.
[6] Gutierrez-Urrutia I, Zaefferer S, Raabe D. Scr Mater 2009;61:737.
[7] Gutierrez-Urrutia I, Zaefferer S, Raabe D. Mater Sci Eng A 2010;527:3552.
[8] Music D, Takahashi T, Vitos L, Asker C, Abrikosov IA, Schneider JM. Appl Phys Lett 2007:91.
[9] Gebhardt T, Music D, Ekholm M, Abrikosov IA, von Appen J, Dronskowski R, et al. Acta Mater 2011;59:1493.
[10] Cankurtaran M, Saunders GA, Ray P, Wang Q, Kawald U, Pelzl J, et al. Phys Rev B 1993;47:3161.
[11] Oliver WC, Pharr GM. J Mater Res 1992;7:1564.
[12] Hohenberg P, Kohn W. Phys Rev B 1964;136:864.
[13] Kresse G, Hafner J. Phys Rev B 1993;48:13115.
[14] Kresse G, Hafner J. Phys Rev B 1994;49:14251.
[15] Schulthess TC, Butler WH, Stocks GM, Maat S, Mankey GJ. J Appl Phys 1999;85:4842.
[16] Spisak D, Hafner J. Phys Rev B 2000;61:11569.
[17] Kresse G, Joubert D. Phys Rev B 1999;59:1758.
[18] Blöchl PE. Phys Rev B 1994;50:17953.
[19] Monkhorst HJ, Pack JD. Phys Rev B 1976;13:5188.
[20] Zunger A, Wei SH, Ferreira LG, Bernard JE. Phys Rev Lett 1990;65:353.
[21] von Appen J, Dronskowski R. Steel Res Int 2011;82:101.
[22] Abrikosov IA, Niklasson AMN, Simak SI, Johansson B, Ruban AV, Skriver HL. Phys Rev Lett 1996;76:4203.
[23] Abrikosov IA, Simak SI, Johansson B, Ruban AV, Skriver HL. Phys Rev B 1997;56:9319.
[24] Cowley JM. J Appl Phys 1950;21:24.
[25] Marinelli P, Baruj A, Guillermet AF, Sade M. Z Metallkd 2000;91:957.
[26] Gavriljuk VG, Sozinov AL, Balanyuk AG, Grigoriev SV, Gubin OA, Kopitsa GP, et al. Metall Mater Trans A 1997;28:2195.
[27] Ledbetter HM, Austin MW. Mater Sci Eng 1985;70:143.
[28] Shanina BD, Gavrilyuk VG, Konchits AA, Kolesnik SP, Tarasenko AV. Phys Status Solidi A – Appl Res 1995;149:711.
[29] Verbeken K, Van Caenegem N, Raabe D. Micron 2009;40:151.
[30] Gebhardt T, Music D, Kossmann D, Ekholm M, Abrikosov IA, Vitos L, et al. Acta Mater 2011;59:3145.
[31] Kooi BJ, Poppen RJ, Carvalho NJM, De Hosson JTM, Barsoum MW. Acta Mater 2003;51:2859.
[32] Nix WD. Mater Sci Eng A 1997;234:37.
[33] Eriksson O. Encyclopedia of materials: science and technology. Amsterdam: Elsevier; 2006.